Aluminium foam with sub-mm sized cells produced using a rotating gas injector

Mike Andreas Noack[a]*, Felix Bülk[a], Ningzhen Wang[a], John Banhart[a,b], Francisco García-Moreno[a,b]

[a] Technische Universität Berlin, Hardenbergstraße 36, 10623 Berlin, Germany

[b] Helmholtz-Zentrum Berlin für Materialien und Energie, Hahn-Meitner Platz 1, 14109 Berlin, Germany

* Corresponding author at: Technische Universität Berlin, Hardenbergstr. 36, 10623 Berlin.
E-mail address: mike.noack@sem.tu-berlin.de.

0 Abstract

Closed-cell solid aluminium alloy foams should ideally contain small and equally sized cells for the sake of better and more predictable mechanical properties, but real foams generated by injection of gas into melts usually exhibit a broad distribution of cell sizes and shapes. Here we investigate how gas bubbles in an aluminium alloy melt containing stabilizing SiC particles can be created in a controlled way by letting the injector move on a circular orbit through the melt at different velocities and adapting the gas flow. The structures of the resulting solidified foams are characterized by X-ray tomography. We identify conditions that allow us to obtain near-monodisperse foams with cell sizes below 1 mm and are able to reduce the content of SiC particles from the usual 20 vol% to 8 vol%.

Keywords: Metal foam; Gas injection; Sub-mm cells; Cell dispersity; Cannula rotation; Tomography

1 Introduction

Aluminium alloy foams are lightweight materials standing out by a combination of low relative density and good mechanical performance. The latter can be improved, e.g. by a smaller variance in density [1–3] as well as a smaller cell size [4]. Gas injection into a metallic melt is a way to produce aluminium foams with closed cells [5–7]. First developments on an industrial

scale included a rotating gas impeller [8, 9]. Such methods were improved by applying different strategies, e.g. varying the compositions of the alloys as well as adding different types and amounts of reinforcing particles [5, 10–14]. It can be shown that added ceramic particles and in-situ produced metal oxides stabilize liquid metal films [10, 15–20]. A process window of stable metal foam in dependence of particle volume fraction and size was shown [10, 20]. Particle additions, however, lead to higher costs in production [21] and potential problems during further (secondary) processing. Therefore, there is an incentive to reduce the fraction of stabilizing particles in the alloy. To produce smaller cell sizes by improving the rate of bubble detachment from the gas injector used the melt with embedded ceramic particles was ultrasonically treated during gas injection in another study in which it was found that gas bubbles detached earlier and therefore smaller bubbles were produced [22]. Alternatively, the gas injector was vibrated vertically [23] or horizontally [11]. Such vibrations in liquid melts, however, induce problems such as a broader variance in cell sizes [11, 22, 23], which might have a negative effect on foam properties and their reproducibility. Monodispersity in metal foams combined with small bubbles could avoid such problems and also lead to bubble crystallization in analogy to aqueous foams [24–26] with associated new properties.

In the present work, we apply a rotating gas injection system intending to improve the bubble detachment rate and reduce the overall cell size of metal foams to below 1 mm of equivalent diameter in combination with a small bubble size dispersion and this with a reduced volume fraction of stabilizing particles.

2 **Experimental**

2.1 Material

A pre-fabricated 40 mm × 20 mm × 80 mm large slab of the commercially available F3S20S alloy from *Alcan, Canada* – AlSi9Mg0.6 (wt%) + 20 vol% SiC particles of 10 µm mean diameter – was used as a precursor for foaming. Similar to the procedure described previously [23], the precursor was remelted in a heatable crucible used for creating foam, see next paragraph. If required, the material was diluted by adding particle-free alloy to the particle

containing melt. The melt was stirred manually using a graphite rod to homogenize the particle distribution [23]. The entire procedure was kept as brief as possible to avoid particle settling.

2.2 Metal foaming setup

Fig. 1 a is a sketch of the gas injection system and its components (the furnace is similar to the one described previously [23]). The furnace consists of a stainless steel base plate framed by two parallel heating plates and two boron nitride plates (front plate in Fig. 1 a is omitted for better visibility) that allow X-ray to pass through and seal the cavity. Altogether, the setup is a closed sealed crucible with an integrated heating. A cylindrical, straight steel cannula with 0.5 mm outer diameter is inserted into the furnace through an alumina tube tightly fitted into an orifice in the steel base plate. The cannula is bent to an angle of 45° after inserting it into the furnace as shown in Fig. 1 b and connected to a rotary gas feedthrough driven by a geared motor. All parts touching the melt consist of boron nitride or are covered in boron nitride spray to reduce possible reactions and aluminium melt adhesion. Heating is controlled by a PID controller with the thermocouple placed at one of the heating plates delivering the actual temperature. The temperature of the melt is measured directly by a thermocouple immersed into the melt. The injection of synthetic air (20.5 vol% O_2) was started after the temperature of the experiment was reached (670 °C in the melt). For low (tangential) cannula tip velocities (v_c<0.4 m·s^{-1}), a pressure-controlled system was used to produce a constant pressure of 1300 mbar. For higher cannula tip velocities a gas flow controller from *voegtlin, Germany* was used with a range of 20–30 ml_n·min^{-1}.

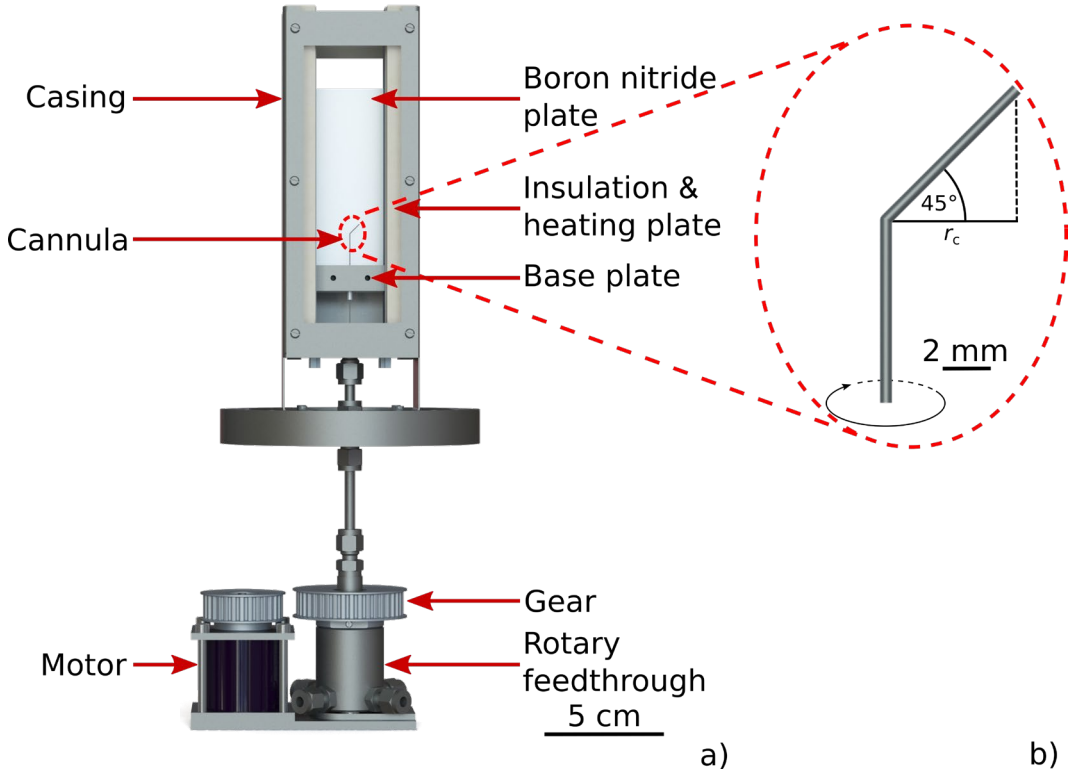

Fig. 1 a – Gas injection setup composed of a furnace combined with a rotary feedthrough and a motor; b – sketch of the bent cannula, with offset of the cannula tip from the rotation axis r_c

2.3 X-ray characterisation

The samples are analysed using a tomography rotation stage from Huber, Germany combined with an X-ray setup similar to the system described previously [23] including a micro-focus X-ray source from *Hamamatsu, Japan* with a conical beam generated by a tungsten target. The applied current and voltage of the source are set to 300 µA and 100 kV, respectively. The transmitted intensities are acquired by a flat panel detector, with 2240 × 2368 pixels and a pixel size of 50 µm, corresponding to an active area of 120 mm × 120 mm, also from *Hamamatsu, Japan.* Due to twofold geometric magnification the effective voxel size for tomography is ~25 µm. For each tomogram, 1001 projections differing by a rotation step width of 0.36 °/image are taken. These images are reconstructed using the software *Octopus 8.8.2* from *Inside Matters, Belgium an*d afterwards quantitatively analysed by the software *AVIZO 9.0.1* from *Thermo Fisher Scientific, USA*. The dispersity as defined by Drenckhan et al. is calculated by [26].

$$\text{Dispersity} = \frac{\text{Standard deviation of equivalent cell diameters}}{\text{Mean value of equivalent cell diameters}} \cdot 100\%, \quad (1)$$

with values of 5% and below defined as monodispersity by Drenckhan et al. [26]. The mean values and standard deviations are obtained by lognormal fitting of histogramms with a bin size of about 0.02 mm as shown in Fig. 2.

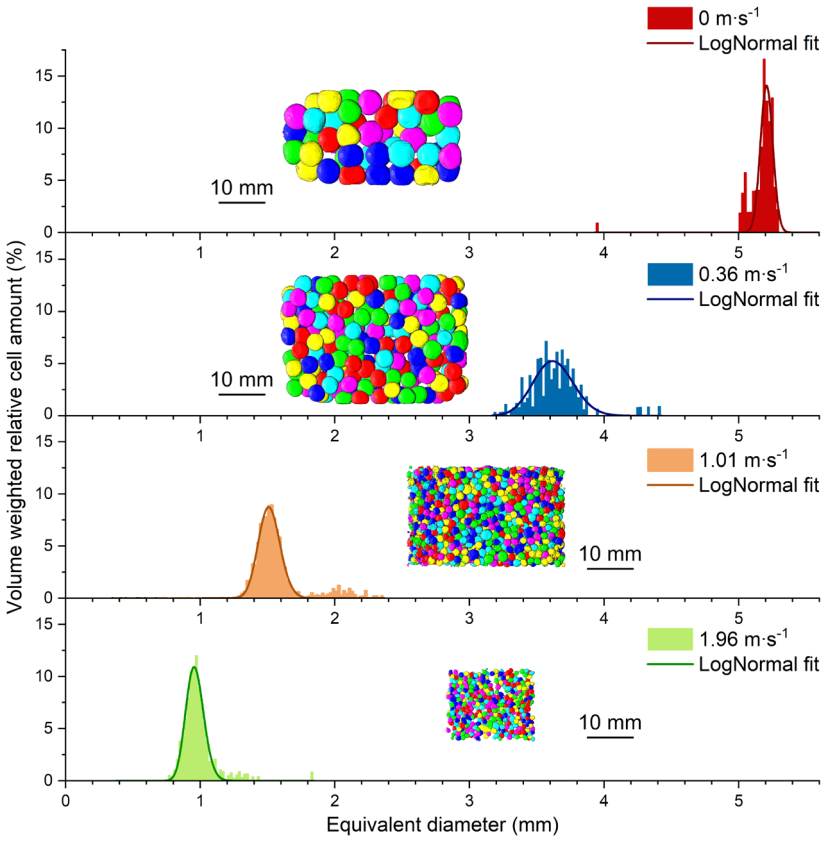

Fig. 2 – Histograms of aluminium foam samples derived from X-ray tomography data with bin size of 0.02 mm. Insets are 3D-rendered images of foams with individually colored cells. Data for four foams produced at four different cannula tip velocities are given (including a resting cannula).

3 Results and Discussion

In Fig. 3, experimental values of the equivalent bubble diameters are shown as a function of the cannula tip velocity. For high particle fractions (20 vol%) and high v_c (>1 m·s^{-1}) no foam was obtained. On the other hand, for low particle volume fractions (8 vol%), no stable foam was observed for low v_c, although Heim et al. indicated stable foam in their static experiments for the same SiC content [20]. Therefore, for higher $v_c \approx 1$ m·s^{-1}, the particle fraction in the melt

was reduced from 20 vol% to 14 vol%, and to 10 vol% ≈1.7 m·s^{-1}. To decrease the cell diameter at ≈2 m·s^{-1} the particle volume fraction was further decreased to 8 vol%.

The mean equivalent cell diameter of the metal foams clearly decreases with rising v_c as shown by tomography, Fig. 3. A reason for this behaviour is that with increasing v_c the drag on the gas bubble increases. According to Wang et al. a higher drag leads to smaller gas bubble sizes [11], further decreases the forces acting on the gas bubble such as the buoyancy force and eventually gives rise to sub-mm sized gas bubbles. Furthermore, a decrease of the applied gas flow rate and particle volume fractions from 10 vol% to 8 vol% also reduce the cell sizes obtained at the same v_c. One reason is a higher resulting effective viscosity for higher particle volume fractions in MMC melts [27]. Additionally, more particles lead to a higher collision rate of particles with a gas bubble [28]. Heim et al. found that particles at a film surface in combination with an oxidation of the film stabilise the film due to inclusion of particles [15]. Furthermore, such particles act as separators between gas bubbles and further stabilize the resulting foam [29, 30].

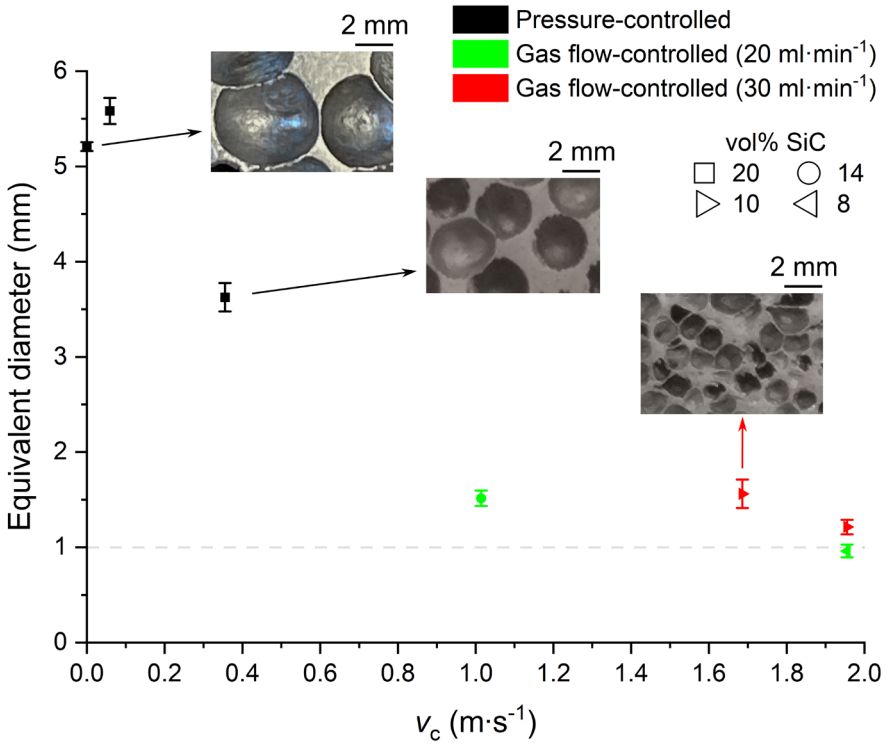

Fig. 3 – Images of the cell structure of aluminium foam samples produced at v_c = 0 m·s^{-1}, 0.36 m·s^{-1} and 1.69 m·s^{-1} as indicated by arrows. Mean equivalent cell diameter in dependence of cannula tip velocity for samples with different SiC content (in vol%) as well as different experimental configurations applied as indicated by differently colored and shaped symbols (pressure-controlled, black; gas flow-controlled 20 ml$_n$·min^{-1}, green; gas flow-controlled, 30 ml$_n$·min^{-1}, red; 20 vol% SiC, squares; 14 vol% SiC, circles; 10 vol% SiC, right-pointing triangles; 8 vol% SiC, left-pointing triangles). The dashed line indicates the 1 mm equivalent diameter target threshold of this study.

As Fig. 4 indicates and Mirsandi et al. have observed by analysing the influence of shear rates on gas bubble geometry [31, 32], the resulting post-mortem-examined cell shape in metallic foams is deformed to elongated with a tail for high v_c. Such tail formation could be caused first by an elongation of the bubble while it is still connected to the cannula as Mirsandi et al. show for aqueous bubbles and simulated for bubbles in a steel melt [31, 32], which is then preserved after detachment by the then oxidised and stabilized inner surfaced that are more rigid than a pure gas/metal interface. Unlike in aqueous systems, gas bubble surfaces in metallic foams are more rigid due to higher melt viscosities and oxidation of the surrounding metallic film, especially if oxygen is contained in the blowing gas [15, 18]. Small resulting standard deviations of cell diameters (<0.09 mm) for $v_c \approx 2$ m·s^{-1} were observed and lead to dispersities

between 6% and 7%, which are close to monodispersity, see Fig 4. A reason for this could be the constant radial acceleration in our rotary system. Wang et al. observed that changes in the cannula tip acceleration (when applying oscillations) lead to a high resulting gas bubble variance if the setup (frequency of cannula movement) is not well synchronized to the gas bubble detachment [11]. The difference in dispersity at the same v_c can be explained by the reduction of the particle content, which leads to a decreasing melt viscosity directly influencing the foam stability [15, 18].

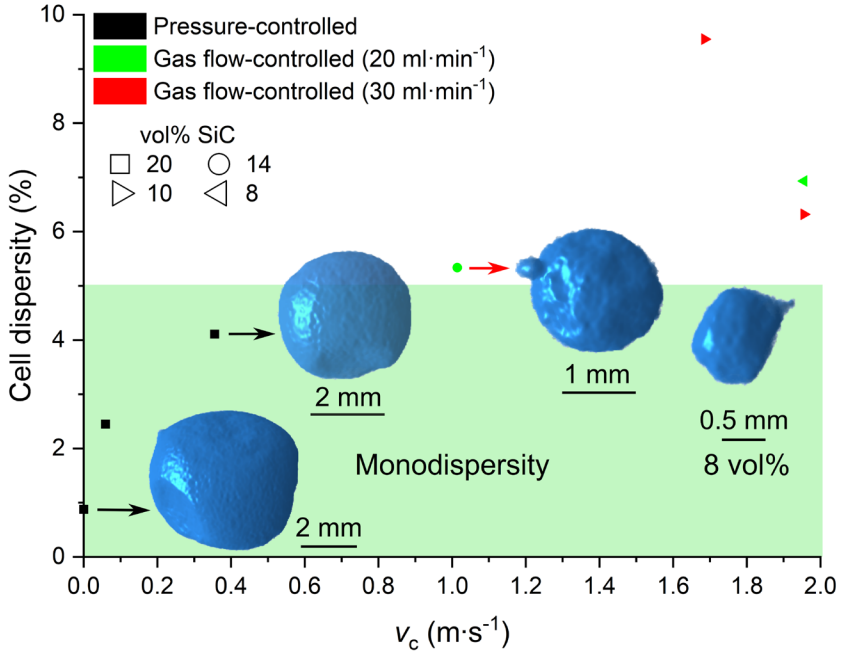

Fig. 4 – Cell dispersity of foams as calculated from Eq. (1) for various different SiC contents differentiated by the experimental configuration applied by differently colored and shaped symbols (pressure-controlled, black; gas flow-controlled 20 mln·min-1, green; gas flow-controlled, 30 mln·min-1, red; 20 vol% SiC, squares; 14 vol% SiC, circles; 10 vol% SiC, right-pointing triangles; 8 vol% SiC, left-pointing triangles). Insets show exemplary gas bubbles of samples foamed at v_c 0 m·s^{-1}, 0.36 m·s^{-1}, 1.01 m·s^{-1} and 1.96 m·s^{-1} as indicated by arrows/labels.

4 Conclusions

AlSi9Mg0.6 (wt%) alloy foams containing up to 20 vol% Si particles were produced by injecting air through a single cannula.

- The large cell size of initially ≈5 mm was reduced to <1 mm by rotating the cannula at a tangential velocity of ≈2 m·s^{-1} and reducing the SiC content to 8 vol%,

- Monodisperse foams were obtained for small cannula tip velocities (<0.4 $m \cdot s^{-1}$) and near-monodisperse foams with mean cell diameters below 1.6 mm (for cannula tip velocities >1 $m \cdot s^{-1}$),
- The technique developed allows us to reduce the particle fraction from initially 20 vol% to 8 vol% SiC while reducing the bubble size and having only a minor impact on bubble size and dispersity.

Acknowledgements

This research was funded by the Deutsche Forschungsgemeinschaft through grants GA 1304/5-1 and BA 1170/35-1.

Data Availability

The experimental data are available from M.A.N. or F.G.M. upon reasonable request.

5 Literature

[1] Banhart, J.: Manufacture, characterisation and application of cellular metals and metal foams. In: Progress in Materials Science 46 (2001) 6, S. 559–632.
[2] Gibson, L. J.; Ashby, M. F.: Cellular solids. Structure and properties, 2. ed., 1. paperback ed. (with corr.), transferred to digital printing. Cambridge 1999.
[3] Andrews, E.; Sanders, W.; Gibson, L. J.: Compressive and tensile behaviour of aluminum foams. In: Materials Science and Engineering: A 270 (1999) 2, S. 113–24.
[4] Wang, N.; Maire, E.; Chen, X.; Adrien, J.; Li, Y.; Amani, Y.; Hu, L.; Cheng, Y.: Compressive performance and deformation mechanism of the dynamic gas injection aluminum foams. In: Materials Characterization 147 (2019), S. 11–20.
[5] Babcsán, N.; Leitlmeier, D.; Degischer, H. P.: Foamability of Particle Reinforced Aluminum Melt. In: Materialwissenschaft und Werkstofftechnik 34 (2003) 1, S. 22–29.
[6] Ashby, M. F.: Metal foams. A design guide. Boston 2000.
[7] Tremblay, F.; Dube, G.: Jet flow device for injecting gas into molten metal, CA19902029680 (1990) CA2029680 (A1).
[8] Jin, I.; Kenny, L. D.; Sang, H.: Method of producing lightweight foamed metal, US19890403588 (1989) US4973358 (A).
[9] Jin, I.; Kenny, L. D.; Sang, H.: Stabilized metal foam body, US19890403588;US19900573716 (1990) US5112697 (A).
[10] Ip, S.: Aluminum foam stabilization by solid particles. In: Canadian Metallurgical Quarterly 38 (1999) 1, S. 81–92.
[11] Wang, N.; Chen, X.; Yuan, J.; Wang, G.; Li, Y.; Zhang, H.; Liu, Y.: Bubble Formation at a Submerged Orifice in High-Speed Horizontal Oscillation. In: Metallurgical and Materials Transactions B 47 (2016) 6, S. 3362–74.

[12] Babcsán, N.; Leitlmeier, D.; Degischer, H. P.; Banhart, J.: The Role of Oxidation in Blowing Particle-Stabilised Aluminium Foams. In: Advanced Engineering Materials 6 (2004) 6, S. 421–28.
[13] Wang, D.; Shi, Z.: Effect of ceramic particles on cell size and wall thickness of aluminum foam. In: Materials Science and Engineering: A 361 (2003) 1-2, S. 45–49.
[14] Vinod Kumar, G. S.; Chakraborty, M.; Garcia-Moreno, F.; Banhart, J.: Foamability of MgAl2O4 (Spinel)-Reinforced Aluminum Alloy Composites. In: Metallurgical and Materials Transactions A 42 (2011) 9, S. 2898–908.
[15] Heim, K.; Vinod Kumar, G. S.; García-Moreno, F.; Rack, A.; Banhart, J.: Stabilisation of aluminium foams and films by the joint action of dispersed particles and oxide films. In: Acta Materialia 99 (2015), S. 313–24.
[16] Wübben, T.; Odenbach, S.: Stabilisation of liquid metallic foams by solid particles. In: Colloids and Surfaces A: Physicochemical and Engineering Aspects 266 (2005) 1-3, S. 207–13.
[17] Kaptay, G.: Interfacial criteria for stabilization of liquid foams by solid particles. In: Colloids and Surfaces A: Physicochemical and Engineering Aspects 230 (2003) 1-3, S. 67–80.
[18] Heim, K.; Kumar, G. V. S.; García-Moreno, F.; Banhart, J.: Role of Ambient Oxygen in the Stabilisation of Single Aluminium Alloy Films. In: Procedia Materials Science 4 (2014), S. 263–68.
[19] Körner, C.: Foam formation mechanisms in particle suspensions applied to metal foams. In: Materials Science and Engineering: A 495 (2008) 1-2, S. 227–35.
[20] Heim, K.; García-Moreno, F.; Banhart, J.: Particle size and fraction required to stabilise aluminium alloy foams created by gas injection. In: Scripta Materialia 153 (2018), S. 54–58.
[21] Bryant, J. D.; Crowley, M.; Wang, W.; Wilhelmy, D.; Kallivayalil, J.: Development of Alcoa Aluminum Foam Products. In: Lefebvre, L. P.; Banhart, J.; Dunand David (eds.): Porous metals and metallic foams. Metfoam 2007 ; proceedings of the Fifth International Conference on Porous Metals and Metallic Foams, September 5 - 7, 2007, Montreal, Canada. Lancaster, Pa. 2008.
[22] Babcsán, N.; Beke, S.; Makk, P.: Method of Producing a Metal Foam by Oscillations and Thus Obtained Metal Foam Product, HU20080000736;WO2009HU00099 (2009) US2011262766 (A1).
[23] García-Moreno, F.; Siegel, B.; Heim, K.; Meagher, A. J.; Banhart, J.: Sub-mm sized bubbles injected into metallic melts. In: Colloids and Surfaces A: Physicochemical and Engineering Aspects 473 (2015), S. 60–67.
[24] García-Moreno, F.; Kamm, P. H.; Neu, T.; Heim, K.; Rack, A.; Banhart, J.: In situ X-ray tomography of aqueous foams: Analysis of columnar foam generation. In: Colloids and Surfaces A: Physicochemical and Engineering Aspects 534 (2017), S. 78–84.
[25] Meagher, A. J.; Whyte, D.; Banhart, J.; Hutzler, S.; Weaire, D.; García-Moreno, F.: Slow crystallisation of a monodisperse foam stabilised against coarsening. In: Soft matter 11 (2015) 23, S. 4710–16.
[26] Drenckhan, W.; Langevin, D.: Monodisperse foams in one to three dimensions. In: Current Opinion in Colloid & Interface Science 15 (2010) 5, S. 341–58.
[27] García-Moreno, F.; Tobin, S. T.; Mukherjee, M.; Jiménez, C.; Solórzano, E.; Vinod Kumar, G. S.; Hutzler, S.; Banhart, J.: Analysis of liquid metal foams through X-ray radioscopy and microgravity experiments. In: Soft matter 10 (2014) 36, S. 6955–62.
[28] Yang, G. Q.; Du, B.; Fan, L. S.: Bubble formation and dynamics in gas–liquid–solid fluidization—A review. In: Chemical Engineering Science 62 (2007) 1-2, S. 2–27.
[29] Banhart, J.: Metal Foams: Production and Stability. In: Advanced Engineering Materials 8 (2006) 9, S. 781–94.

[30] Körner, C.; Arnold, M.; Singer, R. F.: Metal foam stabilization by oxide network particles. In: Materials Science and Engineering: A 396 (2005) 1-2, S. 28–40.
[31] Mirsandi, H.; Smit, W. J.; Kong, G.; Baltussen, M. W.; Peters, E.A.J.F.; Kuipers, J.A.M.: Bubble formation from an orifice in liquid cross-flow. In: Chemical Engineering Journal 386 (2020), S. 120902.
[32] Mirsandi, H.; Baltussen, M. W.; Peters, E.A.J.F.; van Odyck, D.E.A.; van Oord, J.; van der Plas, D.; Kuipers, J.A.M.: Numerical simulations of bubble formation in liquid metal. In: International Journal of Multiphase Flow 131 (2020), S. 103363.